RESCEU-30/99, UTAP-342

# Stochastic Biasing and Weakly Non-linear Evolution of Power Spectrum

Atsushi Taruya

Research Center for the Early Universe (RESCEU), School of Science, University of Tokyo, Tokyo 113-0033, Japan

## ABSTRACT

Distribution of galaxies may be a biased tracer of the dark matter distribution and the relation between the galaxies and the total mass may be stochastic, non-linear and time-dependent. Since many observations of galaxy clustering will be done at high redshift, the time evolution of non-linear stochastic biasing would play a crucial role for the data analysis of the future sky surveys. Recently, analytic study of the time evolution induced by gravity has been reported in the mildly non-linear regime. Here, we further develop the non-linear analysis including the next-to-leading order and attempt to clarify the non-linear feature of the stochastic biasing. Employing the perturbative approach, we compute the one-loop correction of the power spectrum for the total mass, galaxies and their cross correlation. Assuming that the initial distribution of galaxies is given by the local function, we specifically investigate the time evolution of the biasing parameter and the correlation coefficient deduced from the power spectra. On large scales, we find that the time evolution of the biasing parameter could deviate from the linear theory prediction in presence of the initial skewness, even though the scale-dependence of the biasing is very weak. On the other hand, the deviation can be reduced if the stochasticity between the galaxies and the total mass exists. To explore the influence of non-linear gravity, we focus on the quasi-linear scales, where the non-linear growth of the total mass becomes important. It is recognized that the scale-dependence of the biasing dynamically appears and the initial stochasticity could affect the time evolution of the scale-dependence. The result is compared with the recent N-body simulation that the scale-dependence of the halo biasing can appear on relatively large scales and the biasing parameter takes the lower value on smaller scales. Qualitatively, our weakly non-linear results can explain this trend if the halo-mass biasing relation has the large scatter at high redshift.

*Subject headings:* cosmology:theory−large scale structure of universe, galaxies: biasing

## 1. Introduction

Understanding the large scale structure of our universe is the ultimate goal of observational cosmology. Currently, Sloan Digital Sky Survey and Two-Degree Field Survey are working and the enormous observational data will be obtained. In the next generation of deep galaxy surveys, the formation and the evolution of galaxy distribution will be measured more precisely. It provides us with the powerful constraint on the theory of structure formation in the Universe.

When we compare the theoretical prediction for the density fluctuations with the observation of galaxy sky survey, however, the relation between the total mass and the galaxies must be clarified. Since we do not yet have any reliable theory of galaxy/star formation history, there exists the statistical uncertainty between the galaxies and the total mass, which must be determined from the observational data. This uncertainty hampers the effort to obtain the cosmological information such as the density parameter (Hamilton 1998).

Provided the fluctuations of the total mass $\delta_m$ and the distribution of the galaxy number density $\delta_g$, the relation

$$\delta_g = b\ \delta_m \tag{1}$$

is often quoted in the literature. However, the galaxy biasing in nature could be non-linear and the simple linear relation (1) might not be appropriate (Fry & Gaztañaga 1993). Fry (1994) and Gaztañaga & Frieman (1994) compared the observational data with a straightforward extension of (1) given by

$$\delta_g = f(\delta_m) = \sum_{n=1} \frac{b_n}{n!}\ (\delta_m)^n. \tag{2}$$

The assumption (2) still restricts the statistical feature of the galaxy distribution. In general, the relation between the galaxies and the total mass may be time dependent and stochastic (Cen & Ostriker 1992). Therefore, a more general framework to treat this situation is needed, referred to as the stochastic biasing.

Using the different catalogs or subsamples of the galaxy surveys, the observational evidence of stochasticity has been recently discussed (Tegmark & Bromley 1999, Seaborne *et al.* 1999). As for the theoretical study, Dekel & Lahav (1999) has proposed the general formalism for non-linear stochastic biasing. Pen (1998) discussed an observational method to determine the stochasticity. Further, Blanton *et al.* (1998) and Blanton, Cen & Tegmark (1999) performed the cosmological simulation of galaxy formation and demonstrated that the stochastic property of the biasing could evolve due to the galaxy formation process. Since we still lack our knowledge of the non-linear aspect of the stochastic biasing, the qualitative features should deserve consideration .

In this paper, we analytically investigate the dynamical feature of the non-linear stochastic biasing. We study the time evolution induced by gravity, which would be one of the most important sources of non-linearity. The observational study of the galaxy clustering recently shows that the evolution model induced by gravity is sufficient to explain the observed galaxy

distribution at redshift $z < 2$ (Magliocchetti *et al.* 1999, Magliocchetti *et al.* 1999). Therefore, the gravitational evolution of biasing would play a crucial role in the data analyses of future deep sky surveys.

The previous discussion about the time evolution of stochastic biasing has been concentrated on the tree-level analysis, i.e, based on the lowest order perturbation. Tegmark & Peebles (1999) examined the linear evolution. Taruya, Koyama & Soda (1999) has extended the pioneering work of Fry (1996) and investigated the skewness and the bi-spectrum. Taruya & Soda (1999) further study the weakly non-linear galaxy-mass density relation.

This paper focuses on the next-to-leading order of non-linearity. We take into account the one-loop correction of non-linear gravity, corresponding to the one-loop diagram in the graphical representation of perturbation theory (Scoccimarro & Frieman 1996a, 1996b). Then, we shall investigate the power spectrum, the second order statistics of density perturbations in the Fourier space. The power spectrum of the total mass distribution has been extensively investigated by several authors (Makino, Sasaki & Suto 1992, Jain & Bertschinger 1994, Baugh & Efstathiou 1994, Scoccimarro & Frieman 1996b). Our analysis is further extended to the power spectrum of galaxies and the cross correlation between $\delta_m$ and $\delta_g$. Define the vector $\hat{X}^\dagger = (\hat{\delta}_m(\boldsymbol{k}), \hat{\delta}_g(\boldsymbol{k}))$ in the Fourier space, we have the three kinds of power spectrum

$$\langle \hat{X}(\boldsymbol{k}_1)\hat{X}^\dagger(\boldsymbol{k}_2)\rangle = (2\pi)^3\delta_D(\boldsymbol{k}_1+\boldsymbol{k}_2)\begin{pmatrix} P_m(k_1) & P_\times(k_1) \\ P_\times(k_1) & P_g(k_1)\end{pmatrix}, \tag{3}$$

where $P_m(k)$, $P_g(k)$ and $P_\times(k)$ are the power spectrum of the total mass, galaxies and the cross correlation between them. The statistical feature of the galaxy biasing is encoded in the power spectra $P_g(k)$ and $P_\times(k)$, which can be quantified by comparing them with the power spectrum of the total mass distribution. We will analyze the biasing parameter $b_k$ and the correlation coefficient $r_k$ :

$$b_k \equiv \sqrt{\frac{P_g(k)}{P_m(k)}}, \qquad r_k \equiv \frac{P_\times(k)}{\sqrt{P_g(k)P_m(k)}}, \tag{4}$$

which are frequently used in the literature (Tegmark & Peebles 1998, Tegmark & Bromley 1999). Note that the simple biasing prescription (1) restricts the above parameter $r_k = 1$.

We organize the paper as follows; In section 2, we briefly mention the basic formalism for the time evolution of stochastic biasing. The evolution equations (eqs.[6][7] [8]) and the initial conditions (eqs.[12][13]) are presented. Section 3 is devoted to the weakly non-linear analysis. We compute the one-loop correction of the power spectra and the time evolution of the stochastic biasing is investigated in detail. Our main results are described in Section 3.3. We specifically pay attention to the effect of the non-linear biasing (Sec.3.3.1) and the non-linear gravity (Sec.3.3.2). The conclusions and discussion are summarized in section 4.

## 2. Gravitational evolution of Stochastic biasing

Recall the definition of the density field $\delta_m$ and $\delta_g$:

$$\delta_m(x) \equiv \frac{\rho(x) - \bar{\rho}}{\bar{\rho}}, \qquad \delta_g(x) \equiv \frac{n_g(x) - \bar{n}_g}{\bar{n}_g}, \tag{5}$$

where the variables with overbars denote the homogeneous averaged quantity.

The gravitational evolution of the galaxy biasing has been studied by Fry (1996), Tegmark & Peebles (1998) and Taruya, Koyama & Soda (1999). In these papers, the distribution $\delta_m$ follows the equation of continuity and the Euler equation. On the other hand, neglecting the merging and the galaxy formation process, the galaxies are regarded as the test particles in the dark matter distribution $\delta_m$. Thus, the distribution $\delta_g$ should satisfy the equation of continuity whose velocity field is determined by the gravitational potential. On large scales, the assumption of the irrotational velocity flow is valid. We define the velocity divergence $\theta \equiv \nabla \cdot \boldsymbol{v}/(aH)$, where $a$ is the scale factor of the universe and $H$ is the Hubble parameter. The evolution equations for the total mass and the galaxies become

$$\frac{\partial \delta_m}{\partial t} + H\theta + \frac{1}{a}\nabla \cdot (\delta_m \boldsymbol{v}) = 0, \tag{6}$$

$$\frac{\partial \theta}{\partial t} + \left(1 - \frac{\Omega}{2} + \frac{\Lambda}{3H^2}\right) H\theta + \frac{3}{2}H\Omega\delta_m + \frac{1}{a^2 H}\nabla \cdot (\boldsymbol{v} \cdot \nabla)\boldsymbol{v} = 0, \tag{7}$$

$$\frac{\partial \delta_g}{\partial t} + H\theta + \frac{1}{a}\nabla \cdot (\delta_g \boldsymbol{v}) = 0. \tag{8}$$

The variable $\Lambda$ is the cosmological constant and $\Omega$ is the density parameter defined by

$$\Omega \equiv \frac{8\pi G}{3}\frac{\bar{\rho}}{H^2}. \tag{9}$$

Equations (6), (7) and (8) are our basic equations for the time evolution of $\delta_m$ and $\delta_g$. These equations can be solved systematically using the perturbation theory if we give the initial conditions $\delta_{m,g}(x, t_i)$ at an early time $t_i$ order by order. To linear order, provided the initial distributions $\delta_m$ and $\delta_g$ are given in terms of the independent random fields $\Delta_m(x)$ and $\Delta_g(x)$, the solutions become

$$\hat{\delta}_m^{(1)}(x) = D(t)\ \Delta_m(x), \qquad \hat{\delta}_g^{(1)}(x) = \{D(t) - 1\}\,\Delta_m(x) + \Delta_g(x). \tag{10}$$

Since we are interested in the leading behavior of the time evolution, the solutions are only taken into account the growing mode of perturbation denoted as $D(t)$. The function $D(t)$ satisfies

$$\ddot{D} + 2H\dot{D} - \frac{3}{2}H^2\Omega D = 0, \tag{11}$$

with the initial condition $D(t_i) = 1$. Note that the random fields $\Delta_m$ and $\Delta_g$ assign the statistical feature of the galaxies and the total mass. On large scales, the linear perturbation for the

fluctuations $\delta^{(1)}_{m,g}$ may be valid and the central limit theorem implies that the spatial distribution could be well-approximated by the Gaussian statistics. Hence, the variables $\Delta_m$ and $\Delta_g$ are assumed to be the Gaussian random fields.

The full evolution is non-linear, including the higher order perturbative solutions. Regarding the spatial variables $\Delta_{m,g}$ as the seeds of perturbation, the general form of the $n$-th order solutions becomes the terms collecting the time dependent function multiplied by the spatial random variables $[\Delta_{m,g}]^n$. Here, we give the initial distributions $\delta_{m,g}$ as the Taylor expansion of the functions (Taruya, Koyama & Soda 1999, Taruya & Soda 1999)

$$\delta_m(x,t_i) = f(\Delta_m), \qquad \delta_g(x,t_i) = g(\Delta_g). \tag{12}$$

Based on the ansatz (12), we will consider the time evolution emanating from the local biasing. Their functional forms are determined as follows; since the total mass fluctuation is produced during the very early stage of the universe, the gravitational instability induces the deviation from the initial Gaussian distribution. Thus, we give the initial condition of the total mass $f(\Delta_m)$ iteratively from the perturbative solution by dropping the decaying mode. As for the galaxies, the initial distribution $\delta_g$ is induced by the galaxy formation. Currently, it is not feasible to know the initial non-Gaussian distribution $g(\Delta_g)$. We treat $g$ as a parametrized function,

$$g(\Delta_g) = \Delta_g + \frac{h_1}{6}(\Delta_g^2 - \langle\Delta_g^2\rangle) + \frac{h_2}{24}\Delta_g^3 + \cdots. \tag{13}$$

Neglecting the higher order terms, (13) gives the same initial condition as in the linear order solution $\delta^{(1)}_g$.

Notice that the resulting expression for the total mass $\delta_m$ leads to the non-local and non-Gaussian distribution (see eqs.[A-1][A-3]). On the other hand, we simply assume that the function $g(\Delta_g)$ is locally characterized by the constant parameters $h_1$ and $h_2$, which have to do with the initial skewness and initial kurtosis. We should remark that the locality of the galaxy distribution only holds at the initial time. Due to the gravity, the distribution $\delta_g$ can become non-local, which can yield the scale-dependence of the galaxy biasing (Sec. 3.3.2, see also Matsubara 1999).

Once we obtain the perturbative solutions $\delta_{m,g}$, we can investigate the statistical features for the density fluctuations by taking the ensemble average $\langle\cdots\rangle$. In our prescription, the ensemble average is taken with respect to the Gaussian random fields $\Delta_{m,g}$. Their stochasticity is completely characterized by the three quantities. Defining the two-dimensional vector $\hat{Y}^\dagger = (\hat{\Delta}_m, \hat{\Delta}_g)$ in the Fourier space, we have

$$\langle\hat{Y}(\boldsymbol{k}_1)\hat{Y}^\dagger(\boldsymbol{k}_2)\rangle = (2\pi)^3\delta_D(\boldsymbol{k}_1+\boldsymbol{k}_2)\; P_l(k_1)\begin{pmatrix} 1 & b_0\, r_0 \\ b_0\, r_0 & b_0^2 \end{pmatrix}, \tag{14}$$

where the quantity $P_l(k)$ is the initial power spectrum of the total mass. The parameters $b_0$ and $r_0$ are assumed to be the scale-independent variables, for simplicity.

Now, the formalism developed here enables us to obtain the weakly non-linear power spectra (3). Before closing this section, we present the linear order results. Using the relation (14), the three kinds of the power spectra are obtained by substituting the Fourier transform of the linear solutions (10) into the definition (3). Denoting the linear spectrum as $P^{(11)}(k)$, we have

$$\begin{aligned} P_m^{(11)}(k) &= D^2\ P_l(k), \\ P_g^{(11)}(k) &= \left\{(D-1)^2 + 2b_0r_0(D-1) + b_0^2\right\}\ P_l(k), \\ P_\times^{(11)}(k) &= D\left\{(D-1) + b_0r_0\right\}\ P_l(k). \end{aligned} \tag{15}$$

Thus, the biasing parameter $b_k$ and the correlation coefficient $r_k$ can be evaluated from (4) (Tegmark & Peebles 1998, Taruya, Koyama & Soda 1999):

$$b^{(l)}(t) = \frac{\sqrt{(D-1)^2 + 2b_0r_0(D-1) + b_0^2}}{D}, \quad r^{(l)}(t) = \frac{1}{b^{(l)}}\ \frac{D-1+b_0r_0}{D}, \tag{16}$$

where the superscript $(^{(l)})$ means the linear order quantity. The variables $b^{(l)}$ and $r^{(l)}$ are scale-independent and their initial values correspond to the parameters $b_0$ and $r_0$. Note that Fry (1996) has obtained the same result in the specific case $r_0 = 1$. In this case, we immediately obtain $r^{(l)} = 1$ and the relation between $\delta_m$ and $\delta_g$ reduces to the deterministic biasing (1). Thus, in our prescription of the time evolution, the stochasticity in the galaxy biasing comes from the initial condition $r_0 < 1$.

## 3. Perturbative approach to the non-linear power spectra

In this section, we develop the higher order perturbations and investigate the time evolution of galaxy biasing. In section 3.1, the one-loop correction of power spectra is computed. After describing the qualitative feature of the galaxy biasing in the weakly non-linear regime, the time evolution is examined in section 3.3.

### 3.1. One-loop corrections of power spectra

When we take into account the next-to-leading order terms, the power spectrum can be written as

$$P_{(m,g,\times)}(k) = P^{(11)}_{(m,g,\times)}(k) + \left[P^{(22)}_{(m,g,\times)}(k) + P^{(13)}_{(m,g,\times)}(k)\right] + \cdots. \tag{17}$$

The terms in the bracket are the one-loop correction, which can be evaluated using the second and third order solutions of perturbations $\delta_g$ and $\delta_m$. The details of calculation and the resulting expressions for the one-loop spectra $P^{(22)}(k)$ and $P^{(13)}(k)$ are comprehensively described in appendix. Here, we discuss the technical issue to implement the numerical integration.

The expressions for the spectra (A-7)-(A-12) have the three-dimensional integral for the linear power spectra $P_l(k)$. The further reduction enables us to obtain the expressions including the two-dimensional integral over $u$ and $x$ for the $P^{(22)}(k)$ part, while the $P^{(13)}(k)$ part has the one-dimensional integral over $x$ (see appendix). The care is required for evaluation of these integrals. For the single power-law spectrum $P_l(k) \propto k^n$ with $n \leq -1$, the infrared divergence appears at each integral. As for the total mass $P_m^{(22)}(k)$ and $P_m^{(13)}(k)$, which have been studied by several authors, the limit $x \to 0$ yields

$$P_m^{(22)}(k), \quad P_m^{(13)}(k) \ \propto \ k^2 P_l(k) \int_0^\infty dq P_l(q),$$

which imply that the infrared divergences occur at $n \leq -1$. It is known that this is apparent and the divergences cancel out when we evaluate the total contribution of the power spectrum $P_m(k)$ (Makino, Sasaki & Suto 1992, Jain & Bertschinger 1994, Scoccimarro & Frieman 1996b). However, in cases of the power spectra $P_g(k)$ and $P_\times(k)$, the infrared divergences still remain even if we compute the total contribution.

The physical interpretation of the infrared divergence in cases with the single power-law spectrum $P_l(k)$ is difficult. In reality, however, the infrared divergence does not appear if we adopt the phenomenological spectrum such as the Cold Dark Matter (CDM) power spectrum by Bardeen *et al.* (1986), where the effective spectral index $n_{eff} \equiv d \log P_l(k)/d \log k$ becomes positive in the limit $k \to 0$. Therefore, the particular behavior in the single power-law spectrum might not affect the real universe.

On the other hand, depending on the shape of the power spectrum $P_l(k)$, the ultraviolet divergence ($x \to \infty$) appears even in the total mass $P_m(k)$ (Scoccimarro & Frieman 1996b). The integrand from the high frequency part can give the large contribution to the total power spectra and the care is also required to proceed the weakly non-linear analysis self-consistently. Thus, the high-frequency cutoff $k_c$ should be introduced when we evaluate the integrals. If we have the power spectrum $P_l(k)$ as defined with the interval $\epsilon \leq k \leq k_c$, the integral over $x$ and $u$ for the $P^{(22)}(k)$ part and over $x$ for the $P^{(13)}(k)$ part should be replaced:

$$\int_0^\infty dx \longrightarrow \int_{\epsilon/k}^{k_c/k} dx, \qquad \int_{-1}^{1} du \longrightarrow \int_{\mathrm{Max}\{-1,(1+x^2-(\epsilon/k)^2)/(2x)\}}^{\mathrm{Min}\{1,(1+x^2-(k_c/k)^2)/(2x)\}} du. \tag{18}$$

The cutoff $\epsilon$ is auxiliary introduced so that the numerical integration can converge rapidly. As long as the power spectrum $P_l(k)$ has the effective index $n_{eff} > -1$ in the limit $k \to 0$, the influence of the cutoff $\epsilon$ does not affect the weakly non-linear power spectra.

### 3.2. Non-linear biasing and power spectrum

The qualitative features of the one-loop power spectra should be mentioned before analyzing the time evolution. Several authors have discussed the influence of non-linear biasing to the

two-point correlation function (Coles 1993, Fry & Gaztañaga 1993, Scherrer & Weinberg 1998, Heavens, Matarrese & Verde 1998, Dekel & Lahav 1999). The remarkable features appearing in the spectrum of galaxies are summarized as follows :

**(i)** Constant power on very large scales,

**(ii)** Over a wide range of scales, the non-vanishing parameters $h_1$ and $h_2$ modify the biasing parameter $b_k$ predicted in linear theory.

The effect (i) comes from the $P_g^{(22)}(k)$ part of the power spectra. From (A-9), the initial one-loop spectrum $P_g^{(22)}(k)$ becomes

$$\frac{h_1^2}{18} b_0^4 \, \frac{k^3}{(2\pi)^2} \int dx \; x^2 P_l(kx) \; \int du \; P_l(k\sqrt{1+x^2-2xu}).$$

For the typical linear spectrum $P_l(k)$ satisfying the limit $P_l(k) \to 0$ as $k \to 0$, the above integral becomes constant and it eventually dominates over both the linear term $P_g^{(11)}$ and $P_g^{(13)}$ part. This leads to the divergence of the biasing parameter $b_k$ on very large scales.

According to Heavens, Matarrese & Verde (1998), the constant power in the $P_g^{(22)}$ part is interpreted as the shot-noise term, which is a consequence of the local ansatz for the galaxy distribution (see eq.[13]). Although the constant power can be measured on extremely large scales, this would become negligible on realistic scales of the galaxy surveys. Therefore, we will analyze the power spectrum $P_g(k)$ on the scales where the effect (i) becomes negligible.

On the other hand, the clustering of galaxies incorporated by the non-Gaussian initial condition (13) leads to the effect (ii), which would have a more practical importance for the data analysis of galaxy surveys. The dominant contribution of this effect comes from the $P^{(13)}(k)$ part. In our case, the initial biasing parameter is estimated using equation (A-10):

$$b_k \simeq \sqrt{\frac{P_g^{(11)} + P_g^{(13)}}{P_m^{(11)}}} = b_0 \left(1 + \frac{h_2}{8} b_0^2 \; \sigma_0^2\right) \quad ; \quad \sigma_0^2 \equiv \int \frac{d^3\boldsymbol{q}}{(2\pi)^3} \; P_l(q). \tag{19}$$

The expression (19) shows that the deviation from linear theory prediction depends on the parameters $\sigma_0$, $b_0$ and $h_2$. The spectrum $P_l(k)$ with the cutoff parameter implies that the parameter $\sigma_0$ would have the cutoff dependence. In a realistic situation, the clustering property characterized by the assumption (13) might in general depend on the scale. Hence, it is natural to have the cutoff dependence. As for the initial correlation coefficient, it remains unchanged due to the assumption (13). The expressions (A-10) and (A-12) yield

$$r_k \simeq \frac{P_\times^{(11)} + P_\times^{(13)}}{\sqrt{(P_g^{(11)} + P_g^{(13)}) P_m^{(11)}}} = \frac{1 + \frac{h_2}{8} \; b_0^2 \sigma_0^2}{\sqrt{1 + \frac{h_2}{4} \; b_0^2 \sigma_0^2}} \simeq r_0 + \mathcal{O}(\sigma_0^4),$$

which is valid as long as $\sigma_0 \lesssim 1$.

Notice that the gravitational evolution alters the effective biasing and the correlation coefficient. The non-linear biasing parameters $h_1$ and $h_2$ of the one-loop spectra dynamically affect these parameters. Further, the non-linear growth of density fluctuations might change the evolution.

### 3.3. Time evolution of $b_k$ and $r_k$

We now consider the time evolution of the biasing parameter $b_k$ and correlation coefficient $r_k$. In the rest of this paper, we present the results for the linear spectrum $P_l(k)$ given by the standard CDM model. Although we have also examined the two-power-law model of Makino, Sasaki & Suto (1992), we obtained the qualitatively similar results to those shown below. Thus, our results would be general in the case of the realistic spectrum with a break.

From Bardeen *et al.* (1986), the fitting form of the linear spectrum $P_l(k)$ becomes

$$\begin{aligned} P_l(k) &= A\ k\ T^2(k), \\ T(k) &= \frac{\ln(1+2.34q)}{2.34q}\left[1+3.89q+(16.1q)^2+(5.46q)^3+(6.71q)^4\right]^{-1/4}, \\ q &= \frac{k}{\Gamma\ h\ \ \mathrm{Mpc}^{-1}}, \end{aligned} \tag{20}$$

where $k$ is in unit of $h$ Mpc$^{-1}$. We have chosen the shape parameter $\Gamma \equiv \Omega_0 h = 0.5$, corresponding to the parameters $\Omega_0 = 1$ and $H_0 = 100h$ km s$^{-1}$Mpc$^{-1}$ with $h = 0.5$. The linear growing mode $D(t)$ is therefore replaced with $a(t)/a(t_i)$. The cutoff parameters are specified as $\epsilon = 0.0001\ h$ Mpc$^{-1}$ and $k_c = 2\pi/8\ h$ Mpc$^{-1}$, appropriate for examining the weakly non-linear evolution on large scales. Then, the amplitude $A$ is normalized by $\sigma_8 = 0.54$ at the present time ($z = 0$), determined from the cluster abundance (Kitayama & Suto 1997). We then perform the numerical integration for the one-loop corrected terms.

The evolved results of the weakly non-linear power spectra (17) are shown in Figure 1. The thin-solid, thick-solid, and thick-dashed lines are the power spectra $P_m(k)$, $P_g(k)$ and $P_\times(k)$ evaluated at present, respectively. The initial conditions are set at $z = 5$. Choosing the non-Gaussian parameters $h_1$ and $h_2$ as zero, we specify the parameters $b_0 = 3.0,\ r_0 = 0.8$ so that the initial biasing parameter and initial correlation coefficient obtained from (4) become $b_k = 3.0$, $r_k = 0.8$.

In Figure 1, the evolved spectra for galaxies and cross correlation become the larger power than that of the total mass due to the initial large biasing. We have also displayed the linear power spectrum of the total mass $P_m^{(11)}(k)$ (see eq.[15]). Compared to the linear order result, the weakly non-linear spectrum shows the enhancement of the power on small scales, while both $P_m^{(11)}(k)$ and $P_m(k)$ have the same power on large scales. This behavior is known as the weakly non-linear effect (Makino, Sasaki & Suto 1992, Jain & Bertschinger 1994). The validity of the

weakly non-linear result has been checked using the non-linear fitting formula by Peacock & Dodds (1996). The one-loop correction of the total mass rather overestimates the non-linear growth at $z = 0$. However, until $z = 1$, the weakly non-linear spectrum $P_m(k)$ is well-fitted to the formula by Peacock & Dodds and the qualitative behaviors did not change at $z = 0$.

In Figure 2, using the definition (4), we evaluate the biasing parameter $b_k$ and the correlation coefficient $r_k$ as the function of the Fourier mode $k$. Within the validity of the perturbation, the snapshots of both parameters with the same initial conditions as used in Figure 1 are depicted for the different redshift parameters $z = 5, 3, 2$ and 1. On large scales, the spatial dependence of the biasing parameter and the correlation coefficient is very weak and they approach the constant values. The same behaviors can be obtained in the presence of initial non-Gaussianity, consistent with the results by several authors (Mann, Peacock & Heavens 1998, Scherrer & Weinberg 1998, Heavens, Matarrese & Verde 1998). On the other hand, the scale-dependence of the galaxy biasing exists on small scales. Although $b_k$ and $r_k$ initially lose their power due to the high frequency cutoff $k_c$, the spatial variation of the biasing parameter and the correlation coefficient gradually changes.

In the following, we shall separately analyze the time evolution in the linear scale and the quasi-linear scale. Here, the linear scale means that the evolution of the total mass power spectrum can be well-approximated by the linear perturbation (15). The quasi-linear scale denotes the scales where the growth of non-linear correction for the total mass spectrum can become significant, corresponding to $k \gtrsim 0.1\ h\ \mathrm{Mpc}^{-1}$ in Figure 1.

#### *3.3.1. Linear scale*

Since the non-locality of the gravitational evolution does not affect the biasing feature in the linear regime, the scale-independence of $b_k$ and $r_k$ simply relies on the assumption of the local initial conditions (see eq.[13]). We thus analyze the time evolution by fixing the mode $k = 2\pi/100\ h$ $\mathrm{Mpc}^{-1}$. For our purpose, it is important to clarify the influence of the initial non-Gaussianity and the stochasticity to the evolution of $b_k$ and $r_k$. Hence, by varying the non-Gaussian initial parameters $h_1$ and $h_2$, we consider the two cases : almost deterministic biasing ($b_k = 3.0$ $r_k = 0.8$ at $z = 5$) and stochastic biasing ($b_k = 3.0$ $r_k = 0.2$ at $z = 5$). Because the initial non-Gaussianity slightly affects the initial conditions $b_k$ and $r_k$, we appropriately adjust the model parameters $b_0$ and $r_0$ so that the above conditions are satisfied. The list of the model parameters examined in this subsection is shown in Table 1, together with the evolved results $b_k(z = 0)$ and $r_k(z = 0)$. They are compared with the linear prediction (16) under the same initial conditions $b_k$ and $r_k$. The resulting evolution $b_k$ and $r_k$ is depicted in Figure 3a for the nearly deterministic biasing and Figure 3b for the stochastic biasing case. The results are naively extrapolated to the present time $z = 0$.

First, consider the time evolution of the biasing parameter $b_k$. In the deterministic biasing

case (upper panel of Figure 3a), the solid line shows the result with the vanishing initial non-Gaussianity. On the scale $k = 2\pi/100\ h\ \mathrm{Mpc}^{-1}$, there still exists the scale-dependence of the biasing, as shown in Figure 2. This slightly alters the time evolution of $b_k$, compared to the linear prediction $b^{(l)}$ (*thin solid line*). However, this deviation is small and the weakly non-linear evolution is in good accordance with the linear prediction until $z = 1$. The same behavior is obtained in the non-Gaussian initial condition $h_2 = 3.0$ (*dotted line*). Although the non-Gaussian parameter $h_2$ modifies the initial biasing parameter $b_0 = 2.64$ predicted by the linear theory (see eq.[19]), the resulting evolution is well approximated by the linear evolution $b^{(l)}$ with the observed initial condition $b_k = 3.0$ and $r_k = 0.8$.

However, the deviation from the linear evolution is found in the presence of the initial non-Gaussianity $h_1 \neq 0$. The long-dashed and the short-dashed lines are the results with the initial parameter $h_1 = 3.0$ and $h_1 = -3.0$, respectively. In the one-loop power spectrum $P_g^{(13)}(k)$, the terms proportional to the parameter $h_1$ has the time dependence $D^2(t)$ (see eq.[A-10]), which is the same growth rate as appeared in the linear spectrum $P_g^{(11)}$ (see eq.[15]). This means that the clustering property induced by the initial non-Gaussianity tends to remain and the deviation from the linear theory would become increasing. In the $h_1 > 0$ case, we have the positively skewed distribution of galaxies, while the total mass distribution is nearly Gaussian. Thus, the fluctuation $\delta_g$ correlated with the total mass becomes more and more concentrated on the total mass, which dynamically leads to the larger biasing parameter $b_k$. Vice versa, the smaller value $b_k$ could be attained in the case of the initial skewness $h_1 < 0$.

The results of the stochastic biasing case ($b_k = 3.0$, $r_k = 0.2$ at $z = 5$) are displayed in Figure 3b. For the biasing parameter $b_k$ with the initial non-Gaussianity $h_1 \neq 0$, remarkably, the deviation from the linear theory prediction is reduced. From the expressions (A-9) and (A-10), one can show that the one-loop corrected terms proportional to the parameter $h_1$ depends on the multiplicative factor $b_0 r_0$. The small value of the initial correlation coefficient $r_k \simeq r_0$ forces the galaxy distribution to correlate with the total mass. This behavior also affects the galaxy clustering and it can weaken the effect of initial non-Gaussianity. Hence, the biasing parameter $b_k$ could be approximated by the linear theory $b^{(l)}$.

Next, we consider the correlation coefficient. In the bottom panel of Figure 3, we plot time evolution of $r_k$ with the same initial parameters as examined in the upper panel of Figure 3. As was remarked by Dekel & Lahav (1999), the non-linear biasing such as the initial condition (13) can bend the $\delta_g$-$\delta_m$ relation and it effectively decreases the correlation coefficient, compared to the linear result $r_k^{(l)}$. In both panels of Figure 3a and Figure 3b, the effect of non-linear biasing, corresponding to the non-vanishing parameters $h_1$ and $h_2$ is very weak. The time evolution of $r_k$ can be well-approximated by the linear prediction with the initial conditions $b_k = 3.0, r_k = 0.8$ or $b_k = 3.0, r_k = 0.2$.

We have also analyzed the time evolution for more various initial conditions. The examples for the initial anti-biasing case are listed in Table 1. We see that the influence of the initial

non-Gaussianity to the parameters $b_k$ and $r_k$ becomes weak and the linear prediction does work well. In Table 1, the cutoff dependence $k_c$ is also examined. The small value of the cutoff wavelength $2\pi/k_c = 4.35\ h\ \mathrm{Mpc}^{-1}$ increases the parameter $\sigma_0$ given by (19), which strengthens the efficiency of the non-Gaussianity. In particular, the high frequency cutoff with the initial skewness $h_1 = 3.0$ has the curious behavior that the present correlation coefficient $r_k$ becomes larger than unity, which cannot be allowed because the Schwarz inequality states $-1 < r_k < 1$. As for the non-vanishing initial kurtosis $h_2$, we obtain the same present values $b_k$ and $r_k$ as obtained in the cutoff $k_c = 2\pi/8\ h\ \mathrm{Mpc}^{-1}$ case. However, the effective biasing induced by the non-Gaussianity is significant and we have the small value of the initial parameter $b_0 = 2.42$.

### *3.3.2. Quasi-linear scale*

On quasi-linear scales $k \gtrsim 0.1\ h\ \mathrm{Mpc}^{-1}$, the next-to-leading order of non-linear gravity gives the important contribution to the growth of total matter power spectra (see Figure 1).

We pay attention to the non-linear growth, which may be related to the scale-dependence of the biasing shown in Figure 2. From the weakly non-linear analysis $P_m(k)$ by several authors, we have recognized that the mode-mode coupling of long-wave modes contributes to the amplitude of the short-wavelength fluctuations (Makino, Sasaki & Suto 1992). This leads that the power spectrum evolves with the different growth rate, depending on the effective spectral index $n_{eff}$. For the typical spectrum like the CDM model, the one-loop correction causes the significant enhancement of the high-$k$ part of the power spectrum (Jain & Bertschinger 1994).

The weakly non-linear effect also appears in the power spectrum of galaxies $P_g(k)$ and the cross correlation $P_\times(k)$ (see eqs.[A-9]-[A-12]). On appropriately small scales, we could find the enhancement of perturbation $\delta_g$, whose growth rate depends on the initial parameters $b_0, r_0$ and the initial non-Gaussianity, in addition to the effective index $n_{eff}$. Hence, the relative differences between the growth rate of $\delta_g$ and $\delta_m$ dynamically lead to the scale-dependence of the biasing (see Figure 2).

To see the effect of non-linear growth explicitly, we write the parameters $b_k$ and $r_k$ as $b_k = b^{(l)} + b_k^{loop}$ and $r_k = r^{(l)} + r_k^{loop}$. $b_k^{loop}$ and $r_k^{loop}$ are the one-loop correction for the biasing parameter and the correlation coefficient. They are given by

$$
\begin{aligned}
b_k^{loop} &= \frac{b^{(l)}}{2}\left[\frac{P_g^{(22)}(k)+P_g^{(13)}(k)}{P_g^{(11)}(k)} - \frac{P_m^{(22)}(k)+P_m^{(13)}(k)}{P_m^{(11)}(k)}\right], \\
r_k^{loop} &= r^{(l)}\left[\frac{P_\times^{(22)}(k)+P_\times^{(13)}(k)}{P_\times^{(11)}(k)} - \frac{1}{2}\left\{\frac{P_g^{(22)}(k)+P_g^{(13)}(k)}{P_g^{(11)}(k)} + \frac{P_m^{(22)}(k)+P_m^{(13)}(k)}{P_m^{(11)}(k)}\right\}\right].
\end{aligned}
$$

The scale-dependence induced by gravity can be observed from the time evolution of $b_k^{loop}$ and $r_k^{loop}$.

In Figure 4, the snapshots of $b_k^{loop}$ and $r_k^{loop}$ are shown as the function of $k$ for the different redshift $z$. The results at redshift $z = 0$ are also displayed to emphasize the qualitative behavior. In any cases, the scale-dependence of the biasing cannot become significant within the validity of the perturbation theory, however, the scale-dependence obviously exists. The variation of the parameters $b_k^{loop}$ and $r_k^{loop}$ becomes larger on smaller scales.

The characteristic behavior can be recognized in the two cases $b_0 r_0 > 1$ and $b_0 r_0 < 1$, which can be deduced from the one-loop spectrum (A-9)-(A-12). For our qualitative understanding, we simply restrict the analysis on the $h_1 = h_2 = 0$ cases. Figure 4a is the case $b_0 r_0 > 1$, which has the initial condition $b_k = 3.0, r_k = 0.8$ at $z = 5$. Compared to the total mass distribution, the strong clustering of initial galaxies well-correlating with the total mass enhances the non-linear growth of $\delta_g$. Thus, the one-loop correction of the biasing parameter and the correlation coefficient increases in time. On the other hand, the initial distribution $\delta_g$ with the low correlation does not lead to the enhancement of clustering feature, but rather weakens the growth of fluctuations to have the sufficient correlation with the total mass. Figure 4b corresponds to this situation, in which we have chosen the condition as $b_k = 3.0, r_k = 0.2$. Because the growth of perturbation $\delta_m$ becomes larger than that of $\delta_g$, the biasing parameter $b_k^{loop}$ decreases. Interestingly, the one-loop correction $r_k^{loop}$ initially decreases, although the evolution eventually strengthen the correlation.

## 4. Summary and Discussion

In this paper, we have focused on the gravitational evolution of the stochastic galaxy biasing deduced from the power spectrum. Using the perturbation theory, we develop the analysis taking into account the one-loop correction of the non-linear gravity. Assuming the non-local distribution $f(\Delta_m)$ for the total mass and the local initial condition $g(\Delta_g)$ for the galaxy distribution, we examine the weakly non-linear power spectra and investigate the time evolution of biasing parameter and the correlation coefficient. The important conclusions are summarized as follows:

- We found that the initial non-Gaussianity affects the galaxy biasing significantly. In the deterministic biasing, the time evolution of the biasing parameter with the non-vanishing initial skewness deviates from the linear theory prediction by Tegmark & Peebles (1998), even in the linear regime. As time goes on, the deviation cannot be neglected. However, the deviation can be reduced in the presence of the initial stochasticity. On the other hand, the correlation coefficient does not suffer from the initial non-Gaussianity. The time evolution of the correlation coefficient is well-approximated by the linear evolution.

- The local initial condition of the galaxy distribution leads to the almost scale-independent evolution of the biasing on large scales. However, on quasi-linear scales, the one-loop correction of gravity becomes important and it can give the scale-dependence of the biasing. In the typical cases with $b_0 r_0 > 1$ and $b_0 r_0 < 1$, we have the different prediction of the scale-dependence. For the low correlation $b_0 r_0 < 1$, we have the small biasing parameter,

compared with the one on large scales.

The prediction of the scale-dependent biasing just comes from the weakly non-linear results. We cannot say anything about the strong non-linear regime beyond the one-loop correction. However, the weakly non-linear analysis is suitable in investigating the transition from the linear to the non-linear regime. Therefore, our qualitative prediction will not change as long as the gravity plays a role for the scale-dependent biasing. In fact, the halo biasing property taking into account the merging process has recently shown that the biasing parameter decreases as the smoothing scale of density fluctuation becomes small. (Mo & White 1996, Sheth & Lemson 1999, Jing 1998). Further, there is a suggestion that the halo-halo correlation can become anti-biasing on the relatively large scale $k \sim 0.15\ h\ \mathrm{Mpc}^{-1}$ (Kravtsov & Klypin 1999). This indicates that the gravitational clustering gives an important contribution. Therefore, the qualitative behavior can be partially understood from our weakly non-linear analysis.

As a demonstration, we plot the power spectra $P_m(k)$ and $P_g(k)$ at $z = 2.2$ and 0.0 in Figure 5 (*left panel*). The parameters are given at $z = 2.2$, chosen as $b_k = 3.5$, $r_k = 0.1$ and $h_1 = h_2 = 0.0$, i.e, we have the large scatter in the initial $\delta_g$-$\delta_m$ relation. On the scales $k \gtrsim 0.6\ h$ $\mathrm{Mpc}^{-1}$, the perturbation theory breaks down at $z = 0.0$ that the one-loop correction of the total mass dominates the linear order power spectrum $P_m^{(11)}$. However, within the validity domain, the weakly non-linear spectrum $P_g(k)$ decreases its power in the high frequency part and the anti-biasing property appears. This behavior can be illuminated by comparing with the N-body simulation in the right panel of Figure 5, where the spectrum of dark matter particles $P_m(k)$ and halos $P_h(k)$ are presented. The halo and the dark matter catalogue of the simulation are based on the standard CDM model (Magira, Jing & Suto 2000). The halos are identified using the Friend-of-Friends algorithm and selected with the mass threshold $M_{th} = 4.47 \times 10^{12} M_\odot$. Although the halo biasing at $z = 2.2$ is rather larger than the weakly non-linear biasing, the similarities at $z = 0.0$ is apparent. For the detailed comparison, further implementation of our analysis is needed, including the merging process of the halos. The volume exclusion of the halos could be essential for the anti-biasing on small scales. However, the similarities seen in Figure 5 implies that the gravitational evolution and the stochasticity of the galaxy biasing play important role for the present biasing features. We will proceed to improve our treatment quantitatively to explain the halo biasing.

Throughout this paper, we have neglected the galaxy formation. For a realistic situation including this process, the cosmological simulation by Blanton, Cen & Tegmark (1999) shows that the hot gas in the overdense region prevents the star formation and the relation between the galaxies and the dark matter becomes a poor correlation. The realistic process will play a role for explaining the origin of stochasticity. Combining it with our analysis might yield the interesting results.

Potentially, the effective biasing parameter due to the initial non-Gaussianity can cause a serious problem. The determination of the parameters $h_1$, $h_2$ and the correlation coefficient $r_k$

from the observational data would become difficult if there exists the significant contribution of the non-Gaussianity to the galaxy clustering. The method using the higher order correlation (Fry 1994, Gaztañaga & Frieman 1994) should be used carefully, which is partly mentioned by Taruya & Soda (1999). This might lead to a more practical issue, that is, the theoretical prediction of the high redshift objects such as the quasars. In this case, the various cosmological effects should be taken into account. The cosmological redshift distortion and the light-cone effect appeared in the statistical quantities are not negligible for the data analysis (Matsubara & Suto 1996, Yamamoto & Suto 1999). The situation will become more complicated in the case of the biasing being stochastic and non-linear. We shall clarify this issue in the next task.

The author would like to thank Y.Suto for careful reading of the manuscript and stimulating discussions, and J.Soda for suggesting the idea of this work. We are also grateful to H.Magira and Y.P.Jing for providing us the data of the simulation catalog.

## Appendix: Calculation of the one-loop power spectra

In this appendix, we compute the one-loop correction of the power spectra.

We start to obtain the second and the third order solutions of $\delta_m$ and $\delta_g$. To get the solutions, it is convenient to write down the Fourier transform of the evolution equations (6), (7) and (8). The quantities $\delta_m$, $\delta_g$ and $\theta$ are expanded as

$$\delta_{m,g}(x,t) = \int \frac{d^3\boldsymbol{k}}{(2\pi)^3} e^{-i\boldsymbol{k}\boldsymbol{x}}\ \hat{\delta}_{m,g}(\boldsymbol{k},t), \qquad \theta(x,t) = \int \frac{d^3\boldsymbol{k}}{(2\pi)^3} e^{-i\boldsymbol{k}\boldsymbol{x}}\ \hat{\delta}_{m,g}(\boldsymbol{k},t),$$

Then the evolution equations are rewritten with

$$H^{-1}\frac{\partial\hat{\delta}_m(\boldsymbol{k},t)}{\partial t} + \hat{\theta}(\boldsymbol{k},t) = -\int \frac{d^3\boldsymbol{k}'}{(2\pi)^3}\mathcal{P}(\boldsymbol{k}',\boldsymbol{k}-\boldsymbol{k}')\hat{\delta}_m(\boldsymbol{k}-\boldsymbol{k}',t)\hat{\theta}(\boldsymbol{k}',t),$$

$$H^{-1}\frac{\partial\hat{\theta}(\boldsymbol{k},t)}{\partial t} + \left(1-\frac{\Omega}{2}+\frac{\Lambda}{3H^2}\right)\hat{\theta}(\boldsymbol{k},t) + \frac{3}{2}\Omega\hat{\delta}_m(\boldsymbol{k},t)$$
$$= -\int \frac{d^3\boldsymbol{k}'}{(2\pi)^3}\left[\mathcal{P}(\boldsymbol{k}',\boldsymbol{k}-\boldsymbol{k}') + \mathcal{P}(\boldsymbol{k}-\boldsymbol{k}',\boldsymbol{k}') - 2\mathcal{L}(\boldsymbol{k}',\boldsymbol{k}-\boldsymbol{k}')\right]\hat{\theta}(\boldsymbol{k}-\boldsymbol{k}',t)\hat{\theta}(\boldsymbol{k}',t),$$

$$H^{-1}\frac{\partial\hat{\delta}_g(\boldsymbol{k},t)}{\partial t} + \hat{\theta}(\boldsymbol{k},t) = -\int \frac{d^3\boldsymbol{k}'}{(2\pi)^3}\mathcal{P}(\boldsymbol{k}',\boldsymbol{k}-\boldsymbol{k}')\hat{\delta}_g(\boldsymbol{k}-\boldsymbol{k}',t)\hat{\theta}(\boldsymbol{k}',t),$$

where we define

$$\mathcal{P}(\boldsymbol{k}_1,\boldsymbol{k}_2) = 1 + \frac{(\boldsymbol{k}_1\cdot\boldsymbol{k}_2)}{|\boldsymbol{k}_1|^2}, \qquad \mathcal{L}(\boldsymbol{k}_1,\boldsymbol{k}_2) = 1 - \frac{(\boldsymbol{k}_1\cdot\boldsymbol{k}_2)^2}{|\boldsymbol{k}_1|^2|\boldsymbol{k}_2|^2}.$$

Substituting the linear order solutions (10) into the right hand side of the above equations, the second order solutions satisfying the initial conditions become (Fry 1984, Taruya, Koyama & Soda 1999)

$$\hat{\delta}_m^{(2)}(\boldsymbol{k},t) = \int \frac{d^3\boldsymbol{k}_1 d^3\boldsymbol{k}_2}{(2\pi)^3}\ \delta_D(\boldsymbol{k}-\boldsymbol{k}_1-\boldsymbol{k}_2)\ \hat{\Delta}_m(\boldsymbol{k}_1)\hat{\Delta}_m(\boldsymbol{k}_2)\left\{D^2(t)(\mathcal{P}_{1,2}-\frac{3}{2}\mathcal{L}_{1,2}) + \frac{3}{4}E(t)\mathcal{L}_{1,2}\right\}, \tag{A-1}$$

$$\begin{aligned}\hat{\delta}_g^{(2)}(\boldsymbol{k},t) &= \hat{\delta}_m^{(2)}(\boldsymbol{k},t) - \hat{\delta}_m^{(2)}(\boldsymbol{k},t_i)\\ &+ \frac{1}{6}h_1\int \frac{d^3\boldsymbol{k}_1 d^3\boldsymbol{k}_2}{(2\pi)^3}\delta_D(\boldsymbol{k}-\boldsymbol{k}_1-\boldsymbol{k}_2)\left\{\hat{\Delta}_g(\boldsymbol{k}_1)\hat{\Delta}_g(\boldsymbol{k}_2) - (2\pi)^6\langle\hat{\Delta}_g^2\rangle\delta_D(\boldsymbol{k}_1)\delta_D(\boldsymbol{k}_2)\right\}\\ &+ (D(t)-1)\int \frac{d^3\boldsymbol{k}_1 d^3\boldsymbol{k}_2}{(2\pi)^3}\delta_D(\boldsymbol{k}-\boldsymbol{k}_1-\boldsymbol{k}_2)\mathcal{P}_{1,2}\left\{\hat{\Delta}_m(\boldsymbol{k}_1)\hat{\Delta}_g(\boldsymbol{k}_2) - \hat{\Delta}_m(\boldsymbol{k}_1)\hat{\Delta}_m(\boldsymbol{k}_2)\right\},\end{aligned} \tag{A-2}$$

where the expressions $\mathcal{P}(\boldsymbol{k}_1,\boldsymbol{k}_2)$ and $\mathcal{L}(\boldsymbol{k}_1,\boldsymbol{k}_2)$ are respectively suppressed as $\mathcal{P}_{1,2}$ and $\mathcal{L}_{1,2}$. The solutions (A-1) and (A-2) contain the function $E(t)$ which satisfies $E(t_i)=1$. This is the inhomogeneous solution of the following equation:

$$\ddot{E} + 2H\dot{E} - \frac{3}{2}H^2\Omega E = 3H^2\Omega D^2 + \frac{8}{3}\dot{D}^2.$$

In Einstein-de Sitter universe, we have

$$E(t) = \frac{34}{21} D^2(t).$$

It is known that the $\Omega$ and $\Lambda$ dependences of $E/D^2$ is extremely weak (Bernardeau 1994). Therefore, we develop the third order perturbations by replacing $E(t)$ with $(34/21)D^2(t)$. Then we obtain the solutions

$$\begin{aligned}
\hat{\delta}_m^{(3)}(\boldsymbol{k},t) &= D^3(t) \int \frac{d^3\boldsymbol{k}_1 d^3\boldsymbol{k}_2 d\boldsymbol{k}_3^3}{(2\pi)^6}\, \delta_D(\boldsymbol{k}-\boldsymbol{k}_1-\boldsymbol{k}_2-\boldsymbol{k}_3)\, \hat{\Delta}_m(\boldsymbol{k}_1)\hat{\Delta}_m(\boldsymbol{k}_2)\hat{\Delta}_m(\boldsymbol{k}_3) \\
&\quad \times \Big[\frac{7}{18}\mathcal{P}_{1,2}(\mathcal{P}_{3,12}+\mathcal{P}_{12,3}) + \frac{1}{9}(\mathcal{P}_{1,2} - \frac{4}{7}\mathcal{L}_{1,2})(\mathcal{P}_{12,3}+\mathcal{P}_{3,12}-2\mathcal{L}_{12,3}) \\
&\quad\quad - \frac{1}{9}\mathcal{L}_{1,2}(\mathcal{P}_{3,12}+2\mathcal{P}_{12,3})\Big], \qquad \text{(A-3)}
\end{aligned}$$

$$\begin{aligned}
\hat{\delta}_g^{(3)}(\boldsymbol{k},t) &= \hat{\delta}_m^{(3)}(\boldsymbol{k},t) - \hat{\delta}_m^{(3)}(\boldsymbol{k},t_i) \\
&+ \frac{1}{24}h_2 \int \frac{d^3\boldsymbol{k}_1 d^3\boldsymbol{k}_2 d\boldsymbol{k}_3^3}{(2\pi)^6}\, \delta_D(\boldsymbol{k}-\boldsymbol{k}_1-\boldsymbol{k}_2-\boldsymbol{k}_3)\, \hat{\Delta}_g(\boldsymbol{k}_1)\hat{\Delta}_g(\boldsymbol{k}_2)\hat{\Delta}_g(\boldsymbol{k}_3) \\
&+ \int \frac{d^3\boldsymbol{k}_1 d^3\boldsymbol{k}_2 d\boldsymbol{k}_3^3}{(2\pi)^6}\, \delta_D(\boldsymbol{k}-\boldsymbol{k}_1-\boldsymbol{k}_2-\boldsymbol{k}_3) \\
&\times \Big[\mathcal{P}_{3,12}\Big\{-\frac{1}{2}(D(t)-1)\left(\mathcal{P}_{1,2}+\mathcal{P}_{2,1}-\frac{4}{7}\mathcal{L}_{1,2}\right)\hat{\Delta}_m(\boldsymbol{k}_1)\hat{\Delta}_m(\boldsymbol{k}_2)\hat{\Delta}_m(\boldsymbol{k}_3) \\
&\quad + \frac{1}{2}(D(t)-1)^2\mathcal{P}_{1,2}\left(\hat{\Delta}_m(\boldsymbol{k}_1)\hat{\Delta}_g(\boldsymbol{k}_2) - \hat{\Delta}_m(\boldsymbol{k}_1)\hat{\Delta}_m(\boldsymbol{k}_2)\right)\hat{\Delta}_m(\boldsymbol{k}_3) \\
&\quad + \frac{1}{6}h_1\,(D(t)-1)\left(\hat{\Delta}_g(\boldsymbol{k}_1)\hat{\Delta}_g(\boldsymbol{k}_2) - (2\pi)^6\langle\hat{\Delta}_g^2\rangle\delta_D(\boldsymbol{k}_1)\delta_D(\boldsymbol{k}_2)\right)\hat{\Delta}_m(\boldsymbol{k}_3)\Big\} \\
&\quad + \frac{1}{2}\mathcal{P}_{12,3}(D^2(t)-1)\left(\mathcal{P}_{1,2}+\mathcal{P}_{2,1}-\frac{4}{7}\mathcal{L}_{1,2}\right)\hat{\Delta}_m(\boldsymbol{k}_1)\hat{\Delta}_m(\boldsymbol{k}_2)\left(\hat{\Delta}_g(\boldsymbol{k}_3)-\hat{\Delta}_m(\boldsymbol{k}_3)\right)\Big], \qquad \text{(A-4)}
\end{aligned}$$

where the quantities $\mathcal{P}_{ij,l}$, $\mathcal{P}_{l,ij}$ and $\mathcal{L}_{ij,l}$ are respectively given by

$$\mathcal{P}_{ij,l} = \mathcal{P}(\boldsymbol{k}_i+\boldsymbol{k}_j,\boldsymbol{k}_l), \quad \mathcal{P}_{l,ij} = \mathcal{P}(\boldsymbol{k}_l,\boldsymbol{k}_i+\boldsymbol{k}_j), \quad \mathcal{L}_{ij,l} = \mathcal{L}(\boldsymbol{k}_i+\boldsymbol{k}_j,\boldsymbol{k}_l).$$

Using the above results, the one-loop correction for the power spectra can be obtained by taking the ensemble average (14):

Total mass distribution

The one-loop power spectra $P_m^{(22)}(k)$ and $P_m^{(13)}(k)$ are evaluated from the ensemble average

$$\langle\hat{\delta}_m^{(2)}(\boldsymbol{k}_1)\delta_m^{(2)}(\boldsymbol{k}_2)\rangle = (2\pi)^3\delta_D(\boldsymbol{k}_1+\boldsymbol{k}_2)\, P_m^{(22)}(k_1), \qquad \text{(A-5)}$$

$$2\,\langle\hat{\delta}_m^{(1)}(\boldsymbol{k}_1)\delta_m^{(3)}(\boldsymbol{k}_2)\rangle = (2\pi)^3\delta_D(\boldsymbol{k}_1+\boldsymbol{k}_2)\, P_m^{(13)}(k_1). \qquad \text{(A-6)}$$

The results are

$$P_m^{(22)}(k) = \frac{D^4}{2}\int\frac{d^3\boldsymbol{q}}{(2\pi)^3}P_l(q)P_l(|\boldsymbol{k}-\boldsymbol{q}|)\ \boldsymbol{\alpha}^2(\boldsymbol{q},\boldsymbol{k}-\boldsymbol{q}), \tag{A-7}$$

$$P_m^{(13)}(k) = 2\ D^4\ P_l(k)\int\frac{d^3\boldsymbol{q}}{(2\pi)^3}P_l(q)\ \boldsymbol{A}(\boldsymbol{k},\boldsymbol{q},-\boldsymbol{q}), \tag{A-8}$$

which coincide with the weakly non-linear analysis of Makino, Sasaki & Suto (1992), Jain & Bertschinger (1994) and Scoccimarro & Frieman (1996b).

Galaxy distribution

The power spectra $P_g^{(22)}(k)$ and $P_g^{(13)}(k)$ are also given by the ensemble averages (A-5) and (A-6) replacing the subscript $(_m)$ with $(_g)$. The resulting expressions are

$$\begin{aligned}
P_g^{(22)}(k) &= \int\frac{d^3\boldsymbol{q}}{(2\pi)^3}P_l(q)P_l(|\boldsymbol{k}-\boldsymbol{q}|)\\
&\times \Big[\frac{1}{2}(D^2-1)^2\ \boldsymbol{\alpha}^2(\boldsymbol{q},\boldsymbol{k}-\boldsymbol{q})+(D^2-1)(D-1)(b_0r_0-1)\ \boldsymbol{\alpha}(\boldsymbol{q},\boldsymbol{k}-\boldsymbol{q})\boldsymbol{\beta}(\boldsymbol{q},\boldsymbol{k}-\boldsymbol{q})\\
&\quad +(D-1)^2(b_0r_0-1)^2\ \boldsymbol{\gamma}(\boldsymbol{q},\boldsymbol{k}-\boldsymbol{q})+(D-1)^2(b_0^2-2b_0r_0+1)\ \boldsymbol{\epsilon}(\boldsymbol{q},\boldsymbol{k}-\boldsymbol{q})\\
&\quad +\frac{1}{3}h_1(D^2-1)(b_0r_0)^2\ \boldsymbol{\alpha}(\boldsymbol{q},\boldsymbol{k}-\boldsymbol{q})+\frac{1}{3}h_1(D-1)b_0^2r_0(b_0-r_0)\ \boldsymbol{\beta}(\boldsymbol{q},\boldsymbol{k}-\boldsymbol{q})\\
&\quad +\frac{1}{18}h_1^2\ b_0^4\Big]
\end{aligned} \tag{A-9}$$

$$\begin{aligned}
P_g^{(13)}(k) &= 2\ P_l(k)\int\frac{d^3\boldsymbol{q}}{(2\pi)^3}P_l(q)\\
&\times \Big[(D-1+b_0r_0)\Big\{(D^3-1)\ \boldsymbol{A}(\boldsymbol{k},\boldsymbol{q},-\boldsymbol{q})-(D-1)\ \boldsymbol{B}(\boldsymbol{k},\boldsymbol{q},-\boldsymbol{q})\\
&\qquad -(D-1)^2\ \boldsymbol{C}(\boldsymbol{k},\boldsymbol{q},-\boldsymbol{q})+(D^2-1)(b_0r_0-1)\boldsymbol{D}(\boldsymbol{k},\boldsymbol{q},-\boldsymbol{q})\Big\}\\
&\quad +(D-1)^2\Big\{\Big(b_0r_0(D-1)+b_0^2\Big)\boldsymbol{C}(\boldsymbol{k},\boldsymbol{q},-\boldsymbol{q})+b_0^2(r_0^2-1)\boldsymbol{E}(\boldsymbol{k},\boldsymbol{q},-\boldsymbol{q})\Big\}\\
&\quad +\Big\{\frac{1}{3}h_1\ b_0r_0(D-1)+\frac{1}{8}h_2\ b_0^2\Big\}\Big\{(D-1)b_0r_0+b_0^2\Big\}\Big].
\end{aligned} \tag{A-10}$$

Cross correlation

The one-loop power spectra for the cross correlation are computed from

$$\begin{aligned}
\langle\hat{\delta}_g^{(2)}(\boldsymbol{k}_1)\delta_m^{(2)}(\boldsymbol{k}_2)\rangle &= (2\pi)^3\delta_D(\boldsymbol{k}_1+\boldsymbol{k}_2)\ P_\times^{(22)}(k_1),\\
\langle\hat{\delta}_m^{(1)}(\boldsymbol{k}_1)\delta_g^{(3)}(\boldsymbol{k}_2)+\hat{\delta}_g^{(1)}(\boldsymbol{k}_1)\delta_m^{(3)}(\boldsymbol{k}_2)\rangle &= (2\pi)^3\delta_D(\boldsymbol{k}_1+\boldsymbol{k}_2)\ P_\times^{(13)}(k_1).
\end{aligned}$$

Then we have

$$P_\times^{(22)}(k) = \int\frac{d^3\boldsymbol{q}}{(2\pi)^3}P_l(q)P_l(|\boldsymbol{k}-\boldsymbol{q}|)\ \frac{D^2}{2}\ \boldsymbol{\alpha}(\boldsymbol{q},\boldsymbol{k}-\boldsymbol{q})$$

$$\times \quad \left[(D^2-1)\ \boldsymbol{\alpha}(\boldsymbol{q},\boldsymbol{k}-\boldsymbol{q}) + (D-1)(b_0r_0-1)\ \boldsymbol{\beta}(\boldsymbol{q},\boldsymbol{k}-\boldsymbol{q}) + \frac{1}{3}h_1\ (b_0r_0)^2\right] \tag{A-11}$$

$$\begin{aligned} P_{\times}^{(13)}(k) &= P_l(k)\int\frac{d^3\boldsymbol{q}}{(2\pi)^3}P_l(q) \\ &\times \Big[\Big(D(D^3-1)+D^3(b_0r_0+D-1)\Big)\,\boldsymbol{A}(\boldsymbol{k},\boldsymbol{q},-\boldsymbol{q}) - D(D-1)\boldsymbol{B}(\boldsymbol{k},\boldsymbol{q},-\boldsymbol{q}) \\ &\qquad +(b_0r_0-1)D\left\{(D-1)^2\boldsymbol{C}(\boldsymbol{k},\boldsymbol{q},-\boldsymbol{q}) + (D^2-1)\boldsymbol{D}(\boldsymbol{k},\boldsymbol{q},-\boldsymbol{q})\right\} \\ &\quad +D\ b_0r_0\left\{\frac{1}{3}h_1b_0r_0(D-1)+\frac{1}{8}h_2b_0^2\right\}\Big]. \end{aligned} \tag{A-12}$$

The bold-math quantities appeared in the expressions (A-7)-(A-12) are defined as follows:

$$\begin{aligned} \boldsymbol{\alpha}(\boldsymbol{k}_1,\boldsymbol{k}_2) &= \mathcal{P}_{1,2}+\mathcal{P}_{2,1}-\frac{4}{7}\mathcal{L}_{1,2}, \\ \boldsymbol{\beta}(\boldsymbol{k}_1,\boldsymbol{k}_2) &= \mathcal{P}_{1,2}+\mathcal{P}_{2,1}, \\ \boldsymbol{\gamma}(\boldsymbol{k}_1,\boldsymbol{k}_2) &= \mathcal{P}_{1,2}\mathcal{P}_{2,1}, \\ \boldsymbol{\epsilon}(\boldsymbol{k}_1,\boldsymbol{k}_2) &= \frac{1}{2}\left(\mathcal{P}_{1,2}^2+\mathcal{P}_{2,1}^2\right), \\ \boldsymbol{A}(\boldsymbol{k}_1,\boldsymbol{k}_2,\boldsymbol{k}_3) &= \frac{7}{18}\left\{\mathcal{P}_{3,12}\left(\mathcal{P}_{1,2}+\mathcal{P}_{2,1}-\frac{4}{7}\mathcal{L}_{1,2}\right)+\mathcal{P}_{12,3}\left(\mathcal{P}_{1,2}+\mathcal{P}_{2,1}-\frac{8}{7}\mathcal{L}_{1,2}\right)\right\} \\ &\quad +\frac{1}{9}\left(\mathcal{P}_{12,3}+\mathcal{P}_{3,12}-2\mathcal{L}_{12,3}\right)\left(\mathcal{P}_{1,2}+\mathcal{P}_{2,1}-\frac{8}{7}\mathcal{L}_{1,2}\right), \\ \boldsymbol{B}(\boldsymbol{k}_1,\boldsymbol{k}_2,\boldsymbol{k}_3) &= \mathcal{P}_{3,12}\left(\mathcal{P}_{1,2}+\mathcal{P}_{2,1}-\frac{4}{7}\mathcal{L}_{1,2}\right), \\ \boldsymbol{C}(\boldsymbol{k}_1,\boldsymbol{k}_2,\boldsymbol{k}_3) &= \frac{1}{2}\mathcal{P}_{3,12}\left(\mathcal{P}_{1,2}+\mathcal{P}_{2,1}\right), \\ \boldsymbol{D}(\boldsymbol{k}_1,\boldsymbol{k}_2,\boldsymbol{k}_3) &= \frac{1}{2}\mathcal{P}_{12,3}\left(\mathcal{P}_{1,2}+\mathcal{P}_{2,1}-\frac{8}{7}\mathcal{L}_{1,2}\right), \\ \boldsymbol{E}(\boldsymbol{k}_1,\boldsymbol{k}_2,\boldsymbol{k}_3) &= \frac{1}{2}\mathcal{P}_{1,2}\mathcal{P}_{3,12}. \end{aligned}$$

To develop the further evaluation of the one-loop power spectra, we write the integrals in spherical coordinates $q$, $\vartheta$ and $\phi$, where we choose the polar axis aligned with the wave vector $\boldsymbol{k}$. Then we introduce the new variables $x \equiv q/k$ and $u \equiv \cos\vartheta$. The integral over the azimuthal angle $\phi$ simply yields the multiplicative factor $2\pi$ to each one-loop spectrum. As for the integration of $u$, the $P^{(22)}(k)$ part needs the explicit expression of the linear spectrum $P_l(k)$, while we can integrate the $P^{(13)}$ part without knowing the function $P_l(k)$. Thus, using the explicit form $P_l(k)$ given by (20), we numerically evaluate the integral over $x$ and $u$ for the $P^{(22)}(k)$ part. For the $P^{(13)}(k)$ part, the one-dimensional integration over $x$ is only required.

## REFERENCES

Bardeen, J.M., Bond, J.R., Kaiser, N., & Szalay, A.S., 1986, ApJ, 304, 15.

Baugh, C.M., & Efstathiou, G., 1994, MNRAS, 270, 183.

Bernardeau, F., 1994, ApJ, 433, 1.

Blanton, M., Cen, R., Ostriker, J.P., & Strauss, M.A., astro-ph/9807029.

Blanton, M., Cen, R., & Tegmark, M., astro-ph/9903165.

Cen, R., & Ostriker, J.P., 1992, ApJ, 399, L113.

Coles, P., 1993, MNRAS, 262, 1065.

Dekel, A., & Lahav, O., 1999, ApJ, 520, 24.

Fry, J.N., 1984, ApJ, 279, 499.

Fry, J.N., & Gaztañaga, E., 1993, ApJ, 413, 447.

Fry, J.N., 1994, Phys.Rev.Lett, 73, 215.

Fry, J.N., 1996, ApJ, 461, L65.

Gaztañaga, E.,& Frieman, J.A., 1994, ApJ, 437, L13.

Hamilton, A.J.S., 1998, in Proceedings of Ringberg Workshop on Large-Scale Structure, Hamilton, D.(ed.), Kluwer Academic, Dordrecht, p.185.

Heavens, A.F., Matarrese, S., & Verde, L., 1998, MNRAS, 301, 797.

Jain, B., & Bertschinger, E., 1994, ApJ, 431, 495.

Jing, Y.P., 1998, ApJ, 503, L9.

Kitayama, T., & Suto Y., 1997, ApJ, 490, 557.

Kravtsov, A.V., & Klypin, A.A., 1999, ApJ, 520, 437.

Magira, H., Jing, Y.P., & Suto, Y., 2000, ApJ, 528, in press (astro-ph/9907438).

Magliochetti, M., Maddox, S.J., Lahav, O., & Wall, J.V., 1999, MNRAS, 306, 943.

Magliocchetti, M., Bagla, J.S., Maddox, S.J., & Lahav, O., 1999, astro-ph/9902260.

Makino, N., Sasaki, M., & Suto, Y., 1992, Phys.Rev.D, 46, 585.

Mann, B., Peacock, J., & Heavens, A., 1998, MNRAS, 293, 209.

Matsubara, T., 1999, astro-ph/9906029.

Matsubara, T., & Suto, Y., 1996, 470, L1.

Mo, H.J., & White, S.D.M., 1996, MNRAS, 282, 347.

Peacock, J.A., & Dodds, S.J., 1996, MNRAS, 280, L19.

Pen, U., 1998, ApJ, 504, 601.

Seaborne, M.D., Sutherland, W., Tadros, H., Efstathiou, G., Frenk, C.S., Keeble, O., Maddox, S., McMahon, R.G., Oliver, S., Rowan-Robinson, M., Saunders, W., & White, S.D.M., 1999, astro-ph/9905182.

Scoccimarro, R., & Frieman, J.A., 1996a, ApJS, 105, 37.

Scoccimarro, R., & Frieman, J.A., 1996b, ApJ, 473, 620.

Scherrer R.J., & Weinberg, D.H., 1998, ApJ, 504, 607.

Sheth, R.K., & Lemson, G., 1999, MNRAS, 304, 767.

Taruya, A., Koyama., K & Soda, J., 1999, ApJ, 510, 541.

Taruya, A., & Soda, J., 1999, ApJ, 522, 46.

Tegmark, M., & Peebles, P.J.E., 1998, ApJ, 500, L79.

Tegmark, M., & Bromley, B., 1999, ApJ, 518, L69.

Yamamoto, K., & Suto, Y., 1999, ApJ, 517, 1.

Table 1. The list of model parameters used in Figure 3 and the initial conditions $b_k$, $r_k$ given at $z = 5$ for the fixed mode $k = 2\pi/100\ h\ \mathrm{Mpc}^{-1}$. Together with the linear results $b^{(l)}$ and $r^{(l)}$, the present parameters $b_k$ and $r_k$ are also given by extrapolating the weakly non-linear analysis.

| cutoff length | model parameters | | | | $z = 5$ | | $z = 0$ | |
|---|---|---|---|---|---|---|---|---|
| $2\pi/k_c$ $[h^{-1}$ Mpc] | $b_0$ | $r_0$ | $h_1$ | $h_2$ | $b_k$ | $r_k$ | $b_k$ $(b^{(l)})$ | $r_k$ $(r^{(l)})$ |
| 8 | 3.0 | 0.8 | 0.0 | 0.0 | 3.00 | 0.80 | 1.44(1.27) | 0.99(0.97) |
| 8 | 2.93 | 0.82 | 3.0 | 0.0 | 3.00 | 0.80 | 1.69(1.27) | 1.00(0.97) |
| 8 | 2.93 | 0.82 | -3.0 | 0.0 | 3.00 | 0.80 | 1.13(1.27) | 1.00(0.97) |
| 8 | 2.64 | 0.79 | 0.0 | 3.0 | 3.00 | 0.80 | 1.40(1.27) | 0.99(0.97) |
| 8 | 3.0 | 0.20 | 0.0 | 0.0 | 3.00 | 0.20 | 1.03(1.05) | 0.85(0.89) |
| 8 | 2.93 | 0.205 | 3.0 | 0.0 | 3.00 | 0.20 | 1.08(1.05) | 0.85(0.89) |
| 8 | 2.93 | 0.205 | -3.0 | 0.0 | 3.00 | 0.20 | 0.97(1.05) | 0.91(0.89) |
| 8 | 2.64 | 0.199 | 0.0 | 3.0 | 3.00 | 0.20 | 1.02(1.05) | 0.88(0.89) |
| 8 | 0.50 | 0.80 | 3.0 | 0.0 | 3.00 | 0.80 | 0.85(0.91) | 1.00(1.00) |
| 8 | 0.50 | 0.80 | 0.0 | 3.0 | 3.00 | 0.80 | 0.85(0.91) | 1.00(1.00) |
| 4.35 | 2.91 | 0.824 | 3.0 | 0.0 | 3.00 | 0.80 | 1.97(1.27) | 1.05(0.97) |
| 4.35 | 2.42 | 0.782 | 0.0 | 3.0 | 3.00 | 0.80 | 1.41(1.27) | 0.99(0.97) |

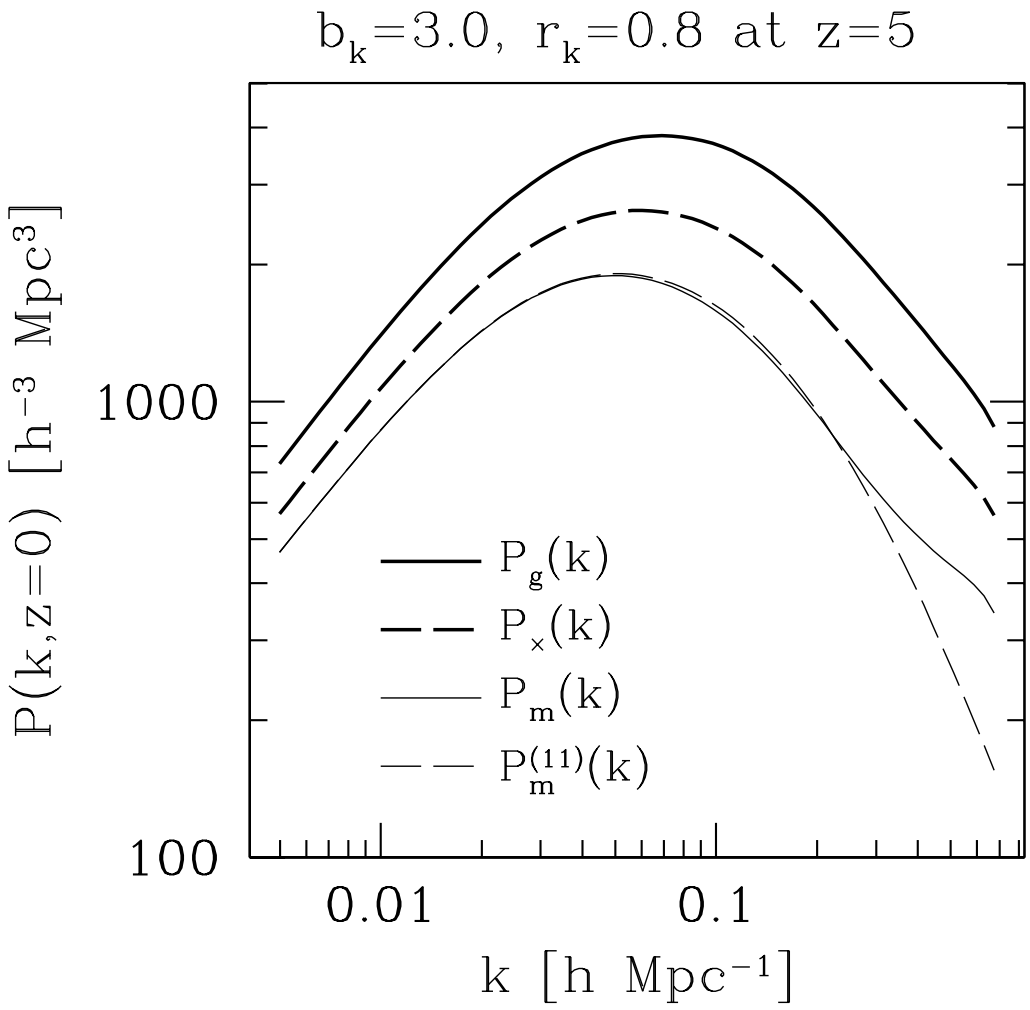


Fig. 1.— The Evolved results of power spectra at $z = 0$. The thin-dashed line shows the linear power spectrum of the total mass $P_m^{(11)}(k)$ evolved from $z = 5$. The initial spectrum is given by the CDM spectrum (20) with the appropriate model parameters (see text). The thin-solid, thick-solid and thick-dashed lines are the weakly non-linear power spectrum of the total mass, galaxies and the cross correlation between them, respectively. The initial conditions at $z = 5$ are specified as $b_0 = 3.0$, $r_0 = 0.8$ and $h_1 = h_2 = 0$.

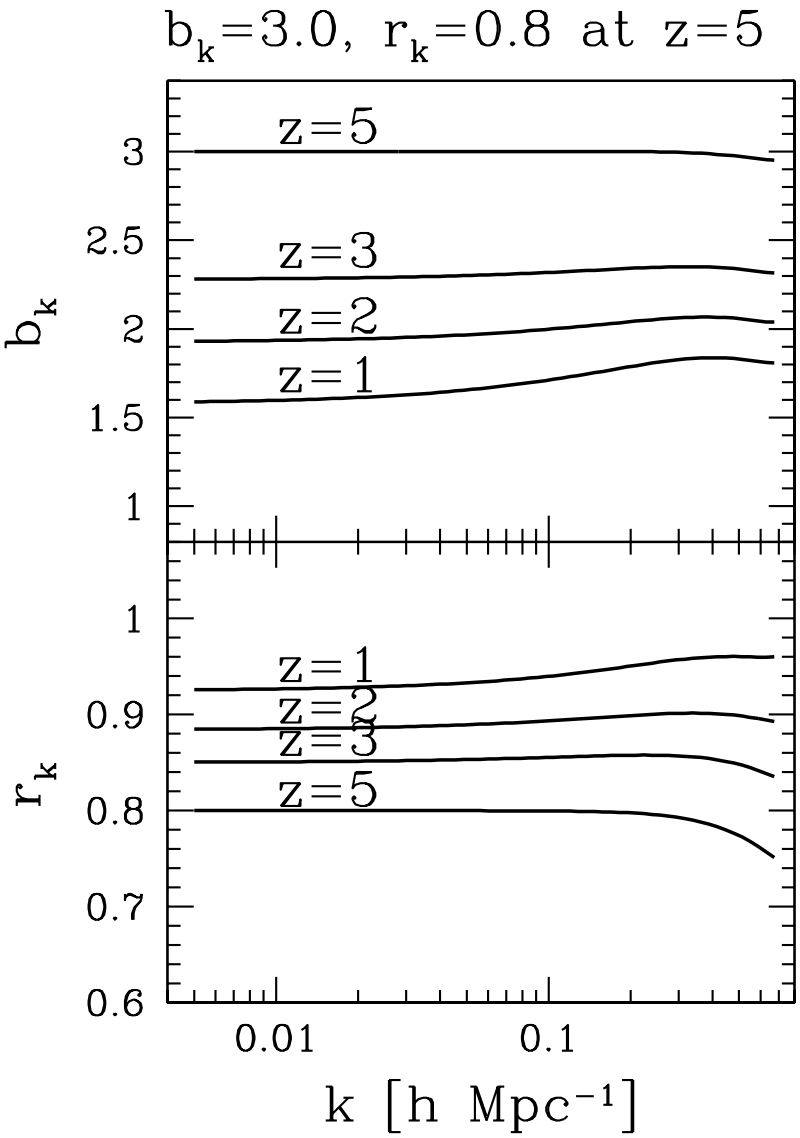


Fig. 2.— The snapshots of the evolved biasing parameter(*upper panel*) and the correlation coefficient(*lower panel*) are depicted as the function of the Fourier mode $k$. The initial condition are the same as in Figure 1. Within the interval $0.001 < k < 0.1\ h\ \ \mathrm{Mpc}^{-1}$, the biasing parameter and the correlation coefficient becomes almost independent of scales.

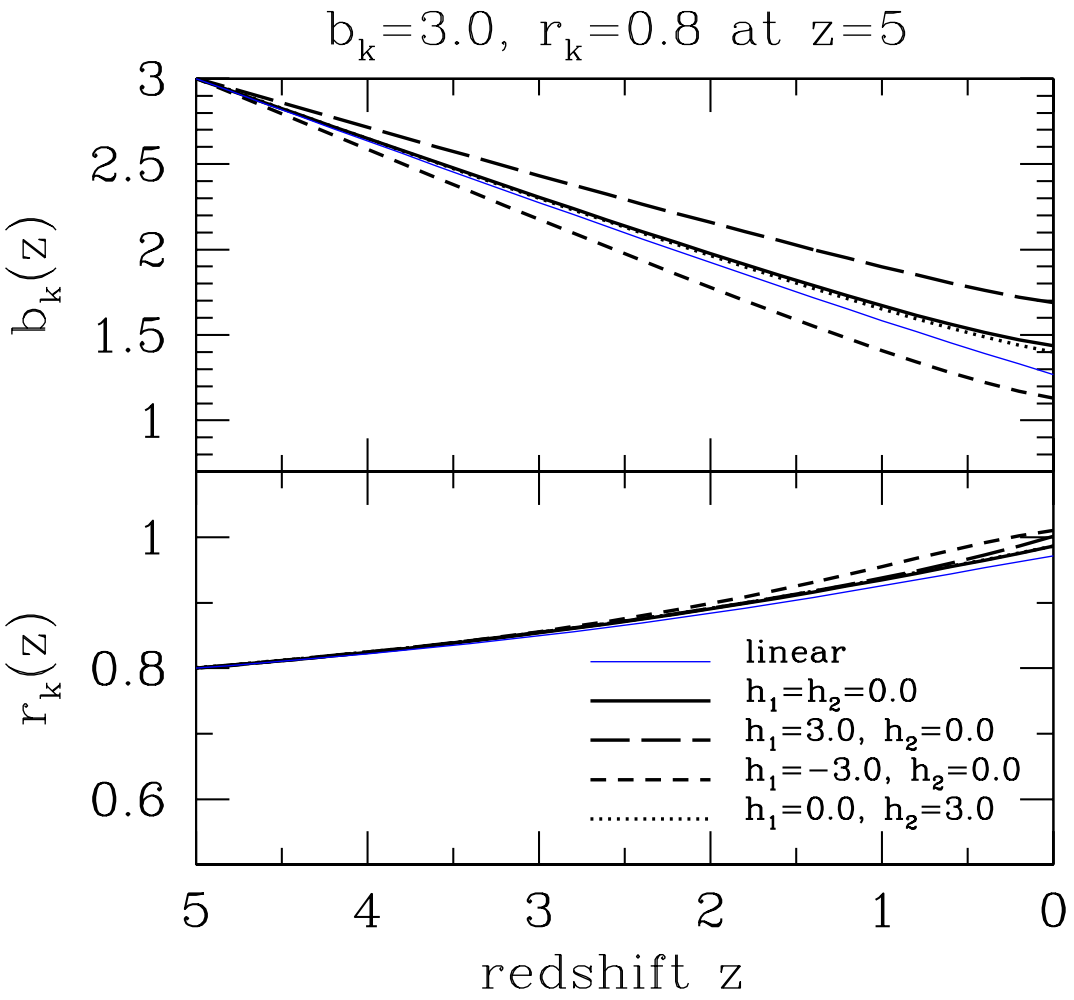


Fig. 3a.— Time evolution of the biasing parameter $b_k$ (*upper panel*) and the correlation coefficient $r_k$ (*lower panel*) as the function of the redshift $z$, fixing the Fourier mode $k = 2\pi/100\ h\ \mathrm{Mpc}^{-1}$. By adjusting the model parameters $b_0$ and $r_0$, the initial conditions at $z = 5$ are specified as $b_k = 3.0$, $r_k = 0.8$, i.e, almost *deterministic biasing case*. The initial non-Gaussianity are respectively chosen as $h_1 = h_2 = 0.0$(*solid line*), $h_1 = 3.0, h_2 = 0.0$(*long-dashed line*), $h_1 = -3.0, h_2 = 0.0$(*short-dashed line*) and $h_1 = 0.0, h_2 = 3.0$(*dotted line*). The results are extrapolated to the present time $z = 0$. For comparison, we also plot the linear result given by (16) with the same initial condition $b_0 = 3.0$, $r_0 = 0.8$ (*thin-solid line*).

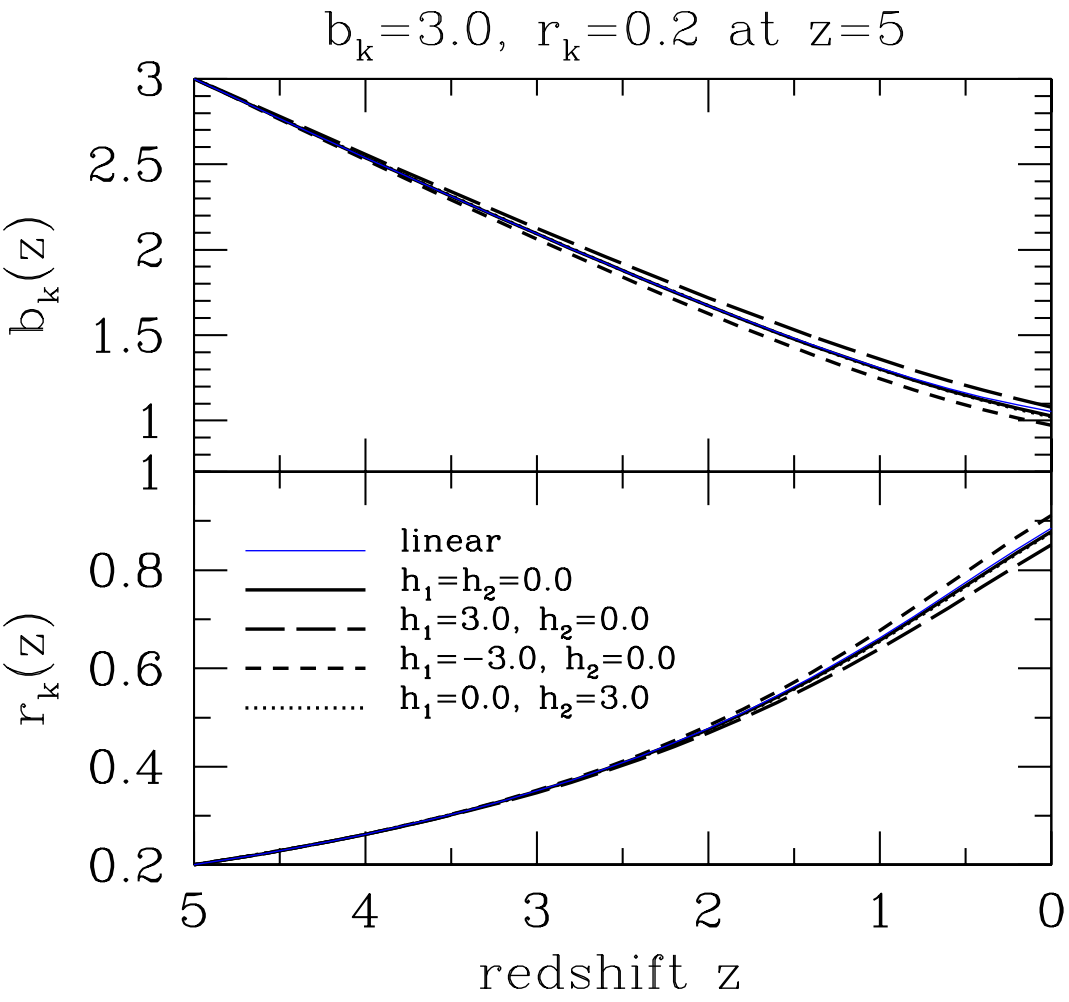


Fig. 3b.— The same figure as in Figure 3a, but with the different initial conditions $b_k = 3.0$, $r_k = 0.2$ (*stochastic biasing case*).

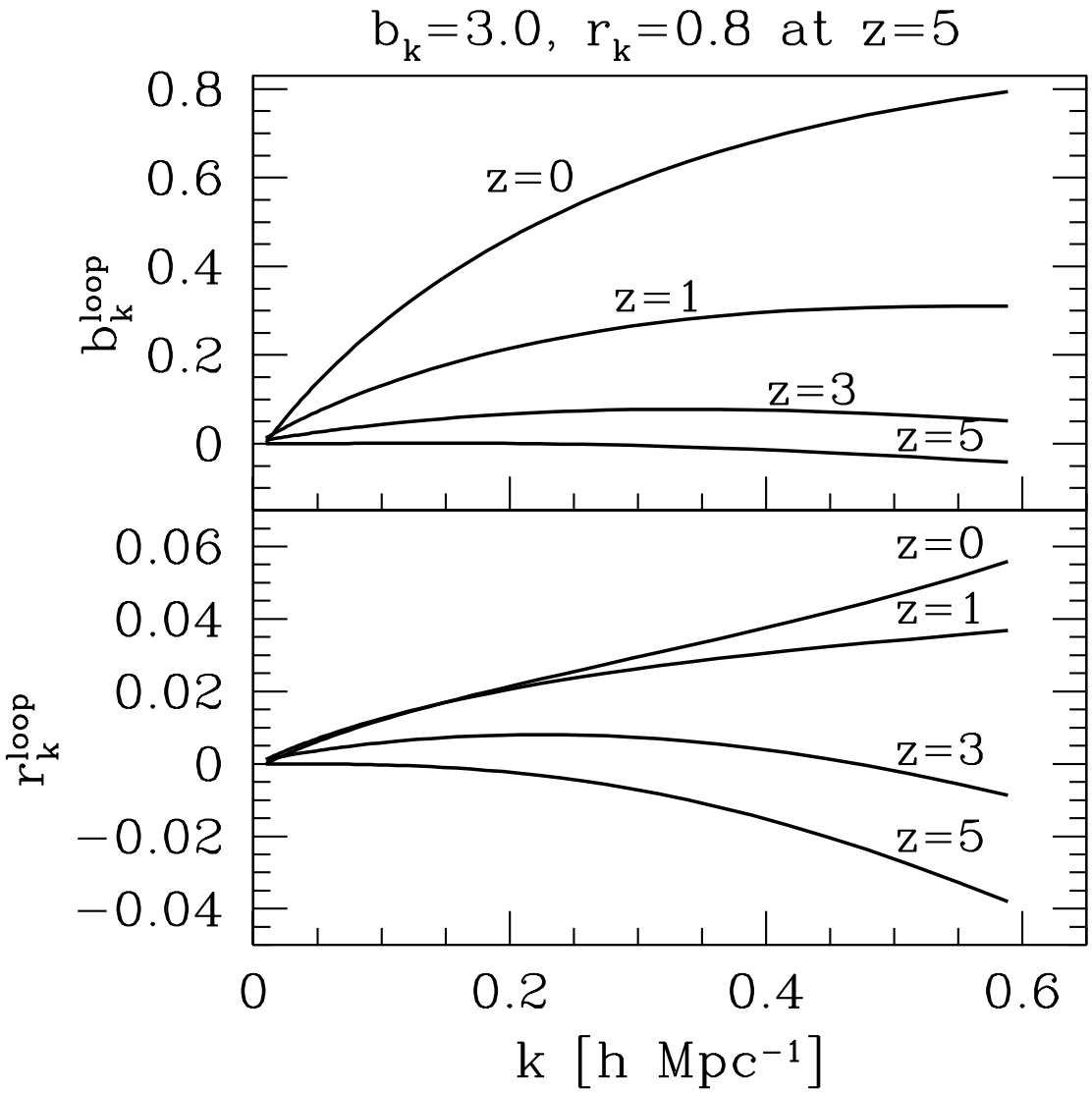


Fig. 4a.— The one loop contribution of the biasing parameter $b_k^{loop}$ and the correlation coefficient $r_k^{loop}$ as the function of the Fourier mode $k$. The initial conditions given at $z = 5$ are specified as $b_k = 3.0$ and $r_k = 0.8$. For simplicity, the initial non-Gaussianity are set by $h_1 = h_2 = 0$. Because of the cutoff $k_c$, the initial parameters $b_k^{loop}$ and $r_k^{loop}$ slightly lose their power at high frequency part. However, it is obvious that the spatial dependence of the parameters $b_k^{(loop)}$ and $r_k^{(loop)}$ dynamically appears. On smaller scales, the spatial variation becomes larger. The typical behaviors are classified as $b_0 r_0 > 1$ (Figure 4a) and $b_0 r_0 < 1$ (Figure 4b).

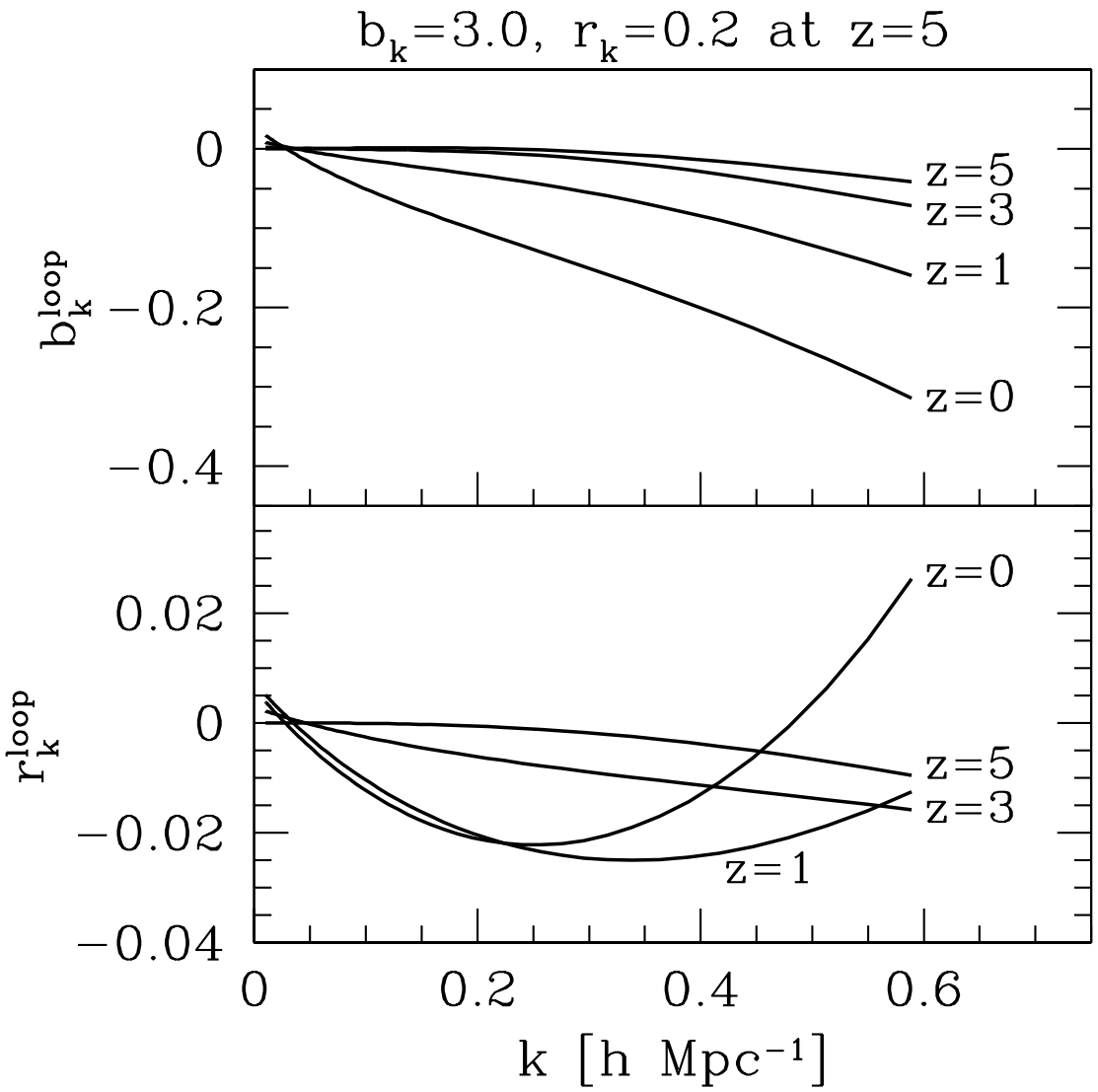


Fig. 4b.— The same figure as depicted in Figure 4a, but with the initial conditions $b_k = 3.0$ and $r_k = 0.2$, corresponding to the $b_0 r_0 < 1$ case.

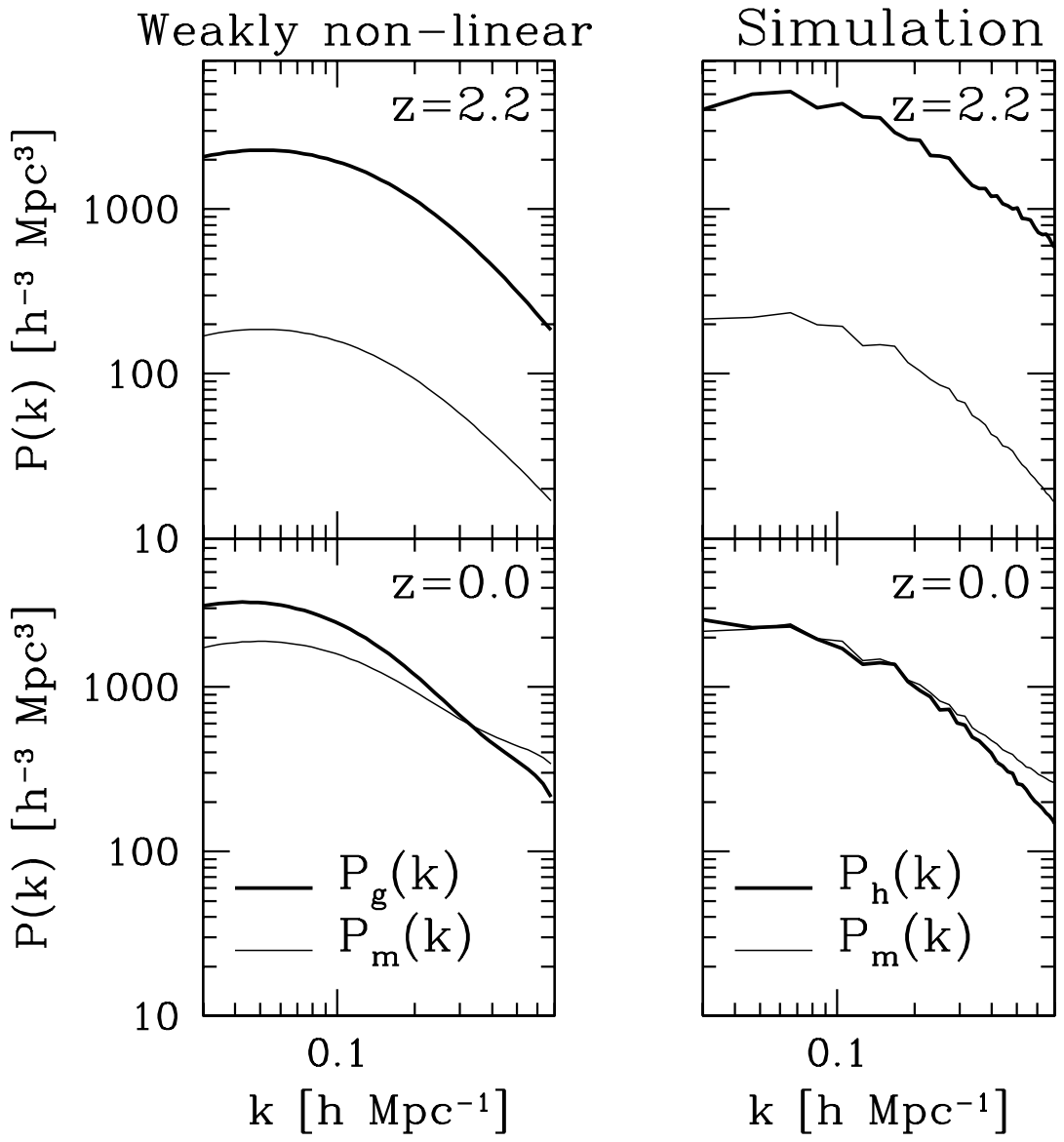


Fig. 5.— The anti-biasing property in the weakly non-linear analysis (*left panel*) and the N-body simulation (*right panel*). In left panel, the weakly non-linear power spectra $P_m(k)$ and $P_g(k)$ are depicted under the initial conditions $b_k = 3.5$, $r_k = 0.1$ and $h_1 = h_2 = 0.0$ given at $z = 2.2$. In right panel, using the simulation catalog of Magira, Jing & Suto (2000), the numerical results of dark matter particles and the halos are presented in the case of Standard CDM model. The halos are identified using the FOF algorithm and selected with the mass threshold $M_{th} = 4.47 \times 10^{12} M_\odot$. Qualitatively, the weakly non-linear result can recover the anti-biasing feature seen in the simulation if the large scatter in the $\delta_g$-$\delta_m$ relation is present initially.